Nuclear Engineering and Technology 54 (2022) 3043–3050

Contents lists available at ScienceDirect

Nuclear Engineering and Technology

journal homepage: www.elsevier.com/locate/net

Original Article

Performance testing of a FastScan whole body counter using an artificial neural network

Moonhyung Cho [a, b, *], Yuho Weon [c], Taekmin Jung [c]

[a] Korea Hydro and Nuclear Power Co., Ltd., 1655, Bulguk-ro, Gyeongju-ci, Gyeongsangbuk-do, Republic of Korea
[b] Department of Nuclear & Quantum Engineering, Korea Advanced Institute of Science and Technology, Republic of Korea
[c] Central Research Institute, Korea Hydro & Nuclear Power Co., Ltd., 70 Yuseong-daero 1312, Beon-gil, Daejeon, 34101, Republic of Korea

ARTICLE INFO

Article history:
Received 23 April 2021
Received in revised form
27 January 2022
Accepted 7 March 2022
Available online 8 March 2022

Keywords:
Internal radioactive contamination
Artificial neural networks
Gamma ray spectroscopy

ABSTRACT

In Korea, all nuclear power plants (NPPs) participate in annual performance tests including *in vivo* measurements using the FastScan, a stand type whole body counter (WBC), manufactured by Canberra. In 2018, all Korean NPPs satisfied the testing criterion, the root mean square error (RMSE) ≤ 0.25, for the whole body configuration, but three NPPs which participated in an additional lung configuration test in the fission and activation product category did not meet the criterion. Due to the low resolution of the FastScan NaI(Tl) detectors, the conventional peak analysis (PA) method of the FastScan did not show sufficient performance to meet the criterion in the presence of interfering radioisotopes (RIs), ^{134}Cs and ^{137}Cs. In this study, we developed an artificial neural network (ANN) to improve the performance of the FastScan in the lung configuration. All of the RMSE values derived by the ANN satisfied the criterion, even though the photopeaks of ^{134}Cs and ^{137}Cs interfered with those of the analytes or the analyte photopeaks were located in a low-energy region below 300 keV. Since the ANN performed better than the PA method, it would be expected to be a promising approach to improve the accuracy and precision of *in vivo* FastScan measurement for the lung configuration.

1. Introduction

Whole body counters (WBCs) are used to measure inhaled or ingested radioisotopes (RIs) of workers in nuclear power plants (NPPs). In Korea, two types of WBCs are used for direct bioassay (*in vivo* counting) at all NPPs. One is the FastScan (stand type), which consists of two large NaI(Tl) detectors, and the other is the AccuScan (bed type), which consists of two HPGe detectors. Although the FastScan has a higher detection efficiency for gamma rays and relatively shorter counting time than the AccuScan, it shows inferior identification and quantification performance due to the low resolution of the NaI(Tl) detectors.

Since 2010, to evaluate the performance of the WBCs used in Korean NPPs, Korea Hydro and Nuclear Power – Central Research Institute (KHNP-CRI) has conducted annual performance tests of the WBCs in accordance with the ANSI/HPS N13.30–2011 Performance Criteria for Radiobioassay, which give three types of testing geometries (lung, total body, and thyroid) for direct radio bioassay performance testing [1]. In 2018, for three out of 13 NPPs, which calibrate the lung configuration as well as the whole body configuration, KHNP-CRI added the lung configuration of the fission and activation product category to the annual performance test. However, the results of the lung configuration for the three NPPs were close to or exceeded the criterion (RMSE $\leq$0.25) given in ANSI/HPS N13.30–2011, while those of the whole body configuration for all NPPs satisfied the criterion [2].

With the development of artificial intelligence technology, artificial neural network (ANN) has been used to overcome the limitation of conventional peak analysis (PA) method in the field of gamma ray spectroscopy. Several published papers have used ANNs as an alternate identification or quantification method for low resolution gamma ray spectrometers [3–6]. However, there have been no papers applying ANNs to assess intake of RIs for NPP workers.

In this study, we have developed an ANN as the quantification method to improve the performance of the FastScan in the lung configuration. In addition, we propose a quantification method of converting the activity ratio to the amount of activity, because the

* Corresponding author. Korea Hydro and Nuclear Power Co., Ltd., 1655, Bulguk-ro, Gyeongju-ci, Gyeongsangbuk-do, Republic of Korea.
E-mail address: chomh9525@khnp.co.kr (M. Cho).

https://doi.org/10.1016/j.net.2022.03.008

outputs of the ANN are not the amount of activity but the relative activity of RIs in a sample. This results from that the activation function of the output layer of the ANNs is a softmax function which ranges from 0 to 1. Based on the quantification result, we have carried out a performance test using our developed ANN and compared its performance to the results of the PA method that is currently used to quantify the results of the FastScan.

2. Materials and methods

2.1. Equipment

2.1.1. FastScan

The FastScan, shown in Fig. 1, is designed to quickly monitor (e.g., in less than 3 min) the internal contamination of radiation workers in NPPs. The dual NaI(Tl) detector design of the FastScan provides a uniform response along the longitudinal axis from the thyroid of the tallest 99th percentile male to the lower gastrointestinal (GI) tract of the shortest female [7].

2.1.2. RMC-II phantom

A Radiation Management Corporation (RMC-II) phantom (see Fig. 2) was developed by Canberra Inc. to closely approximate the source/absorber configurations specified by ANSI/HPS N13.30 as appropriate for WBC calibration. The phantom consists of two components: a “torso” section, which includes three interior source cavities providing the lung, whole body and G.I. equivalent configurations, and a “neck” section for the thyroid configuration [8].

Before any spectra were measured, the RMC-II phantom was positioned on a stool at a height of 76 cm in the WBC shield according to the manufacturer's recommendation.

2.1.3. Standard radioisotopes

To test the performance of the FastScan in accordance with ANSI/HPS N13.30–2011, six standard RIs were manufactured and their activities were certified by the Korea Research Institute of Standards and Science (KRISS). Table 1 shows the RIs used in the performance test of the lung configuration, the minimum testing level (MTL) given in ANSI/HPS N13.30–2011, and the certified activity.

Fig. 1. The FastScan (manufactured by Canberra).

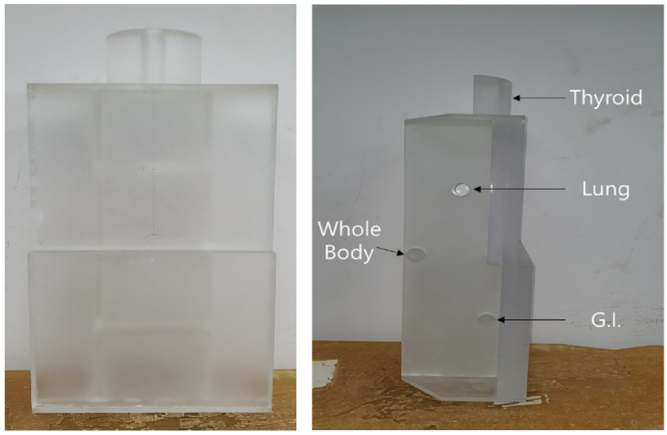

Fig. 2. Front (on the left) and side (on the right) views of the RMC-II transfer phantom.

Fig. 3 shows the normalized spectra of the six standard RIs measured by the FastScan at KHNP-CRI. Prior to measure each RI, the FastScan was calibrated using a reference material certified by the KRISS. Eq. (1) is the energy calibration result that decides the relation between the channel and energy (E) in x-axis, and Eq. (2) is FWHM (Full- Width at Half Maximum) calibration result that establishes the relation between the peak width and energy.

$$E = 4.48 + 1.925 \cdot ch + 1.71E - 04 \cdot ch^2 \quad (1)$$

$$FWHM = -10.398 + 2.303\sqrt{E} \quad (2)$$

2.2. Overview of ANN

2.2.1. Peak analysis vs. ANN

There are some differences in the analysis of RIs between the ANN presented in this work and the conventional PA method that is currently used with the FastScan for gamma ray spectroscopy. Table 4 summarizes and compares the two methods.

Table 1
Details of the RIs used in the performance test.

RIs	Gamma rays		MTL[a] (kBq)	Activity[b] (kBq)
	Energy(keV)	Emission rate		
^{54}Mn	835	1	3	5.93
^{57}Co	122	0.855	3	6.77
	136	0.107		
^{58}Co	511	0.299	3	6.59
	811	0.994		
^{60}Co	1173	1	3	6.18
	1332	1		
^{134}Cs[c]	563	0.083	–	6.72
	569	0.154		
	605	0.976		
	796	0.855		
^{137}Cs[c]	662	0.85	–	5.97

[a] The upper bound of the testing range shall not exceed 20 times the stated MTL.
[b] The activity of the highest and lowest testing RIs in any one test phantom shall be within a factor of three of each other.
[c] These RIs shall be present in the phantom in appropriate amounts for interference but shall not be tested.

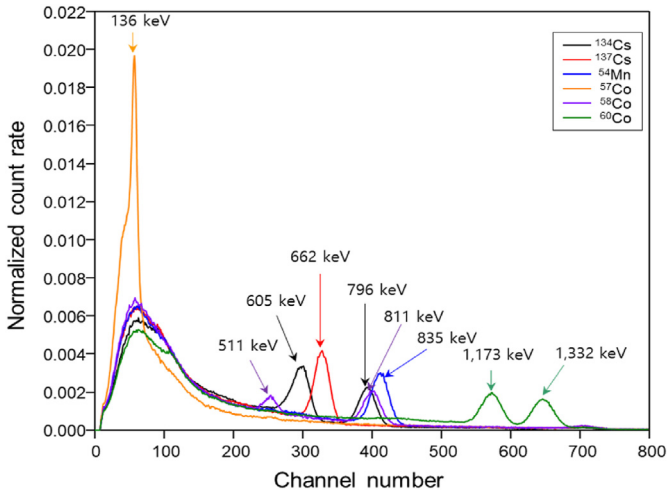

Fig. 3. Normalized spectra of the six standard RIs measured by the FastScan.

Table 2
Six test datasets.

RIs	Case					
	1	2	3	4	5	6
^{54}Mn	○	○	○			
^{57}Co	○			○	○	
^{58}Co		○		○		○
^{60}Co			○		○	○

2.2.2. Neural networks

ANNs are often used in machine learning. An ANN is a brain-inspired mathematical framework that is used to learn representations from data [9]. An ANN is comprised of an input layer, hidden layers, output layer, all of which are interlinked and contain several neurons as shown in Fig. 4 [3].

The components and basic functions of an ANN are as follows:

- Input layer: The very first layer of the ANN. Training data is entered into the input layer.
- Hidden layer: Any layer between the input and output layer. Each hidden layer receives weights from the input layer or previous layer, and then sends its output to the next hidden layer or output layer.
- Output layer: The last layer of the ANN, which produces the output.
- Neuron: A basic information processing unit in a neural network. Fig. 5 shows the operation of a single neuron. Input vector **A** of ANN is weighted by weight vector **W.** The weighted sum becomes the input of an activation function (f) that computes the output of the neurons. The output is transferred to the next layer and it becomes an element of the input vector **C.** By changing weight vectors according to the true values, ANN can minimize the gap between the output of ANN and the true values.

In this study, a rectified linear unit (ReLU) function, shown in Eq. (3) is used as the activation function of input and hidden layers. For the output layer, the softmax function, shown in Eq. (4), is used because it is the most suitable function in classification and has been proven to show good performance for RI identification and quantification [3].

$$relu(x) = \max(0, x) \tag{3}$$

$$softmax(z_j) = \frac{\exp(z_j)}{\sum_{k=1}^{K}\exp(z_k)} \tag{4}$$

During training of an ANN, the weights of the neurons in each layer are adjusted to minimize the cost functions using a process called backpropagation which recalculates the weights and biases for each neuron. The cost function used in this study is cross entropy [3].

$$E = -\frac{1}{N}\sum_{n=1}^{N} y_n \log(\hat{y}_n) + (1 - y_n)\log(1 - \hat{y}_n) \tag{5}$$

Where N is the total number of output nodes, y_n is the truth of the nth output, and $\hat{y}_n$ is the ANN output of the nth output.

A new weight w_j^{new}, which reduces the cost function, can be calculated using a gradient descent algorithm that finds the gradient of the cost functions [4]. The equation for w_j^{new} is

$$w_j^{new} = w_j^{old} + \Delta w_j \tag{6}$$

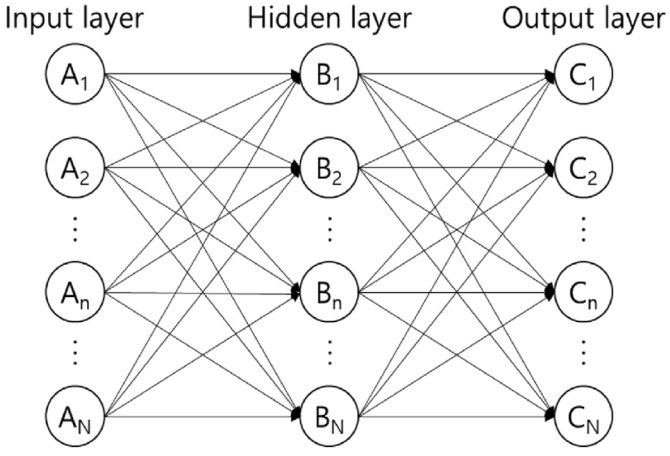

Fig. 4. Example of an ANN (input layer: A, hidden layer: B, output layer: C).

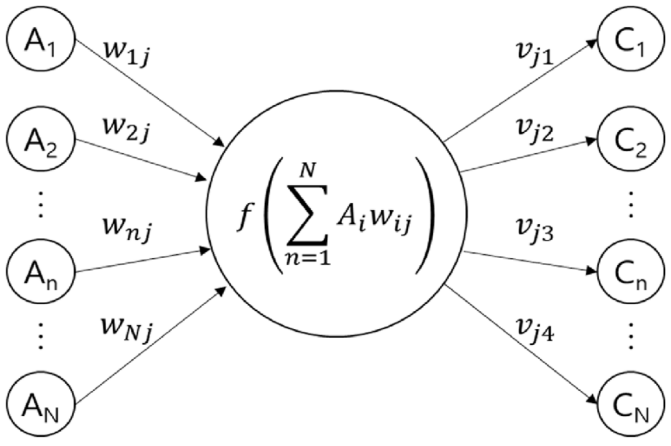

Fig. 5. The operation of a single neuron.

$$\Delta w_j = -\eta \frac{dE}{dw_j} \quad (7)$$

where η is the learning rate of the ANN.

When an ANN reaches an ideal level of performance, the gradient approaches 0 and the difference between the predictions of the ANN and the actual values may be very small.

2.3. Creation of datasets

2.3.1. Training and validation datasets

Training and validation datasets are used to fit the parameters (e.g., weights) and tune the hyper-parameters (e.g., number of layers or neurons) during the learning process [10]. In previous studies, creating a dataset of real gamma ray spectra was deemed to be so impracticable that simulated spectra created using computer codes(e.g., GADRAS or MCNP6) or synthetic spectra were instead used to train ANNs [3,4]. In this work, synthetic spectra, S, are created as training and validation datasets because they are relatively easy to make, less time consuming, and more realistic than computer codes.

$$S = \sum_{i=1}^{N} \varepsilon_i \cdot y_i \cdot r_i \cdot B_i \quad (8)$$

where N is the number of RIs, ε_i is the efficiency of the detector (i.e., net count rate per gamma rays), y_i is the gamma ray emission rate per decay, r_i is the relative activity contribution of the RIs, and B_i is the base spectrum (i.e., normalized spectrum) of the RIs to be trained [5].

To make the base spectra, each RI was inserted into the cavity of the lung configuration of the RMC-II phantom and counted for 1,800 s. Using Eqs. (8), 50,000 and 5,000 synthetic spectra were created for the training and validation sets, respectively. The amount of the data sets in this study would be enough if the RMSE values derived by the ANN satisfy the criterion, RMSE $\leq$0.25.

2.3.2. Test data sets

Test datasets, which are independent of the validation datasets, are used only once to assess an ANN model because tuning of the hyper-parameters through the repeated use of the validation datasets may leak some information about the validation datasets to the ANN model [9]. The test datasets used to evaluate the performance of the ANN are the actual spectra of each RI measured in the FastScan, not by synthesizing the base spectra. Here, the measurement time of the actual spectra is set to 1 min because the measurement time of the FastScan in Korea NPPs is normally set to 1 min. Each RI was measured five times, which is the minimum number of replicates required for a performance test according to ANSI N13.30–2011. Two interfering RIs, ^{134}Cs and ^{137}Cs, and any two RIs among ^{54}Mn, ^{57}Co, ^{58}Co, and ^{60}Co were selected to satisfy the test condition given in ANSI N13.30–2011. Table 2 shows the six cases that resulting from the combination ($_4C_2 = 6$) of the two RIs that can be selected from the RI set. The two interfering RIs, ^{134}Cs and ^{137}Cs, are included in all the cases.

Fig. 6 shows an example of a comparison of the synthetized spectrum with measured spectrum for 1 min for Case 3.

The relative activity contributions, r_i, for synthetizing ^{54}Mn, ^{60}Co, ^{134}Cs, ^{137}Cs are 0.1, 0.31, 0.24, and 0.35, respectively. As shown in Fig. 6, the synthetic spectrum mimics the measured spectrum well enough to be used for the training and validation of the ANN.

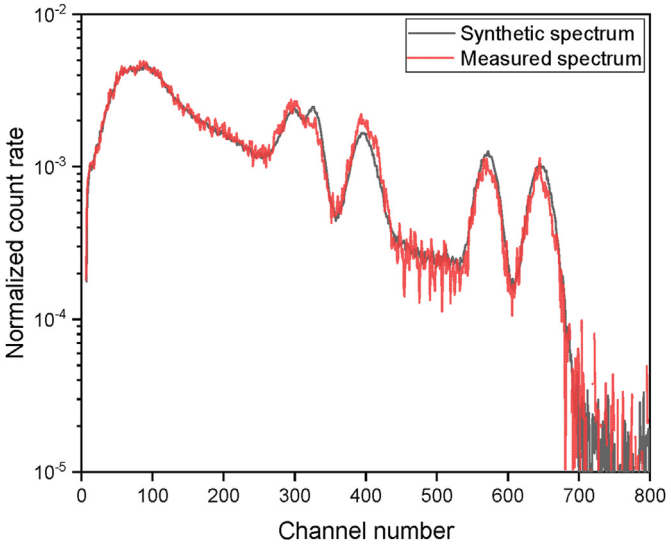

Fig. 6. Comparison of the synthetized spectrum with measured spectrum for 1 min for Case 3.

2.4. Hyperparameter optimization (HPO)

Hyperparameters refer to the variables which determine the structure of an ANN and how the ANN is trained. For example, the former includes the number of hidden layers and the number of nodes in each hidden layer, while the latter includes the learning rate, batch size, activation functions, etc. Identification of the optimum hyperparameters can enhance the performance of an ANN. Various algorithms are used for the HPO (e.g., grid search, random search, Bayesian search, etc.). In this work, Bayesian optimization, one of the automated HPO methods, is used because it is more computationally efficient at finding the optimum hyperparameters compared with grid or random search. Bayesian optimization in this study is implemented by using the Gaussian process of the Python package, Scikit-optimize.

The selected hyperparameters, range of the hyperparameters, and optimized hyperparameter values which produce the best accuracy (about 97%) on validation datasets for the ANN presented in this work are given in Table 3.

2.5. Quantification of activity from the ANN output

To calculate the B_r, S_B, and RMSE values for the performance test, the output of the ANN resulting from use of the softmax function should be converted from relative activity to the amount of the activity of an individual RI in a sample. This can be done as follows:

The net count rate is calculated by subtracting the background count rate from the gross count rate. The net count rate (x cps) of a spectrum can be expressed as

Table 3
Range of hyperparameter search spaces and optimized values according to Bayesian search.

Hyperparameters	HP Range	Optimized HP Values
Number of hidden layers	1–5	2
Number of neurons in hidden layer 1	10^2–10^3	546
Number of neurons in hidden layer 2	10^2–10^3	828
Learning rate	10^{-4} - 10^{-2}	$1.35x10^{-3}$
Batch size	30–500	64

Table 4
Summary of the differences between the ANN and PA method.

	ANN	PA method
Nuclide identification	Uses the activity ratio which exceeds a pre-determined threshold	Uses the peak search algorithm, energy calibration result, and nuclide library
Features used for quantification	Entire spectrum (including Compton continuum)	Part of spectrum (i.e., photopeak region)
Quantification method	Predicts activity ratio with a trained ANN	Corrects count rate with an efficiency calibration curve

$$x\ \text{cps} = \sum_{i=1}^{N} A_i \cdot \varepsilon_i \cdot y_i \tag{9}$$

where A_i is the activity of the ith RI, which is unknown and ε_i and y_i are the efficiency and gamma ray emission rate, which are the same variables given in Eq. (8). Because the output of the ANN is the relative activity contribution in a sample, A_i can be expressed as

$$A_i = \frac{r_i}{r_j} A_j \tag{10}$$

where A_j is the activity of the RI, r_i is the relative activity contribution of A_i, and r_j is the relative activity contribution of A_j.

For example, if we quantify the amount of activity of A_1 from the output ($N = 6$) of the ANN, the activity of the other five RIs can be expressed using Eq. (10).

$$A_2 = \frac{r_2}{r_1} A_1,\ A_3 = \frac{r_3}{r_1} A_1,\ A_4 = \frac{r_4}{r_1} A_1,\ A_5 = \frac{r_5}{r_1} A_1,\ A_6 = \frac{r_6}{r_1} A_1$$

By inserting the values of A_2 to A_6 into Eq. (9), we can solve for A_1

$$A_1 = \frac{x\ \text{cps}}{\sum_{i=1}^{N} \frac{r_i}{r_1} \cdot \varepsilon_i \cdot y_i}$$

Using the same procedure, the other five RIs can also be quantified.

2.6. Performance criterion

The performance of the FastScan is evaluated by the root mean square error (RMSE) of relative bias and precision according to ANSI N13.30–2011. To be acceptable, the RMSE shall be less than or equal to 0.25. RMSE is calculated as follows [1]:

$$RMSE = \sqrt{B_r^2 + S_B^2} \le 0.25 \tag{11}$$

2.6.1. Relative bias

Relative bias, B_r, is a measure of how close the assessed activity is to the actual activity. It is calculated as the average in the individual relative bias statistic [1].

$$B_r = \sum_{i=1}^{N} \frac{B_{ri}}{N} \tag{12}$$

where N is the number of measurements and B_{ri} is a relative bias statistic defined for the purpose of performance testing of a finite number of measurements [1].

$$B_{ri} = \frac{(A_i - A_{ai})}{A_{ai}} \tag{13}$$

where A_i is the assessed value of the ith measurement of RIs and A_{ai} is the actual activity of the RIs. For convenience, absolute values of B_r are used in this study.

2.6.2. Relative precision

The relative precision of the measurement process represents the relative dispersion of the values of B_{ri} from the mean B_r; It is defined as follows [1]:

$$S_B = \sqrt{\frac{\sum_{i=1}^{n} (B_{ri} - B_r)^2}{(N-1)}} \tag{14}$$

2.6.3. Decision of net count rate of the PA method

In the PA method mentioned by the manual of the manufacturer, Canberra Inc., the left and right limits of ROI (Region of Interest) are determined by 1.25 FWHM of the peak area and then the left and right boundary of the ROI are determined by the X-point average algorithm provided by Genie 2000 software. After deciding the ROI, the net count rate, which is gross peak area minus background continuum under the peak area, is calculated by Sum/Non-Linear Least Squares Fit Peak Area algorithm provided by the same software [11].

3. Results and discussion

To calculate the RMSE values of the ANN results, activity ratios, which are the outputs of the ANN, were converted to the amount of the activity using Eqs. (9) and (10). For example, Table 5 shows the outputs of the ANN for Case 1 and the net count rates calculated from the spectra. Activity ratios of less than 0.05 were considered false positives. In Table 5, the ratios for ^{58}Co and ^{60}Co are missing because they provided the data for the case.

Using Eq. (9), the efficiency (ε_i) values for ^{54}Mn, ^{57}Co, ^{58}Co, ^{60}Co, ^{134}Cs, and ^{137}Cs were 0.041, 0.025, 0.041, 0.04, 0.04, and 0.043, respectively, and the gamma ray emission rates y_i given in Table 1 were used for each RI.

Table 6 shows the converted activities for ^{54}Mn corresponding to the values in Table 5, as well as a comparison of the performance

Table 5
The ANN outputs and net count rate for Case 1.

No	Activity ratio						Net count rate
	^{54}Mn	^{57}Co	^{58}Co	^{60}Co	^{134}Cs	^{137}Cs	
1	0.211	0.192	0.010	0.001	0.286	0.300	1,010
2	0.211	0.199	0.000	0.000	0.286	0.303	1,003
3	0.213	0.201	0.000	0.000	0.285	0.302	1,001
4	0.216	0.201	0.000	0.000	0.285	0.298	1,005
5	0.215	0.198	0.000	0.000	0.285	0.302	1,001

Table 6
Performance comparison (ANN vs. PA method) for ^{54}Mn in Case 1.

No	Activity (Bq)		Relative bias statistic (B_{ri})	
	ANN	PA method	ANN	PA method
1	4,267	3,251	0.008	0.235
2	4,217	3,973	0.004	0.061
3	4,235	3,865	0.001	0.087
4	4,324	3,607	0.022	0.147
5	4,282	4,098	0.012	0.031
Relative bias (B_r)			0.008	0.112
Relative precision (S_B)			0.010	0.080
RMSE			0.013	0.137

test between the ANN and PA methods. In this case, the RMSE value of the ANN is about 10 times lower than that of the PA method.

All the outputs of the ANN were converted to the amount of the activity using the procedure discussed above and the activity according to the PA method were referred to the analysis reports of the FastScan.

To compare performance between the ANN and PA method for the six cases shown in Table 2, relative bias (B_r), relative precision (S_B), and RMSE values were calculated. The results are depicted as histograms in Figs. 7–9, respectively. In Fig. 7, the horizontal red line shows the limit of the criterion.

Table 7 shows the numerical RMSE values derived using the two methods, which are depicted in Fig. 7.

In all cases, the RMSE values of the ANN have met the criterion, while some of the RMSE values derived from the PA method were close to or exceeded the criterion. The RMSE values of the ANN range from 0.008 to 0.214; these values are lower than those of the PA method, which range from 0.054 to 0.321. The maximum RMSE value produced by the ANN was 0.214 for ^{57}Co in Case 1, which satisfies the criterion, while that of the PA method is 0.321 for ^{57}Co in Case 5, which exceeds the criterion. The performance of the ANN is superior to that of the PA method, except for in three instances, ^{57}Co in Case 1, ^{60}Co in Case 3, and ^{58}Co in Case 5, which show little disparity between the two methods.

We classified the results of the performance test into three categories based on the energy range of the RIs that were tested.

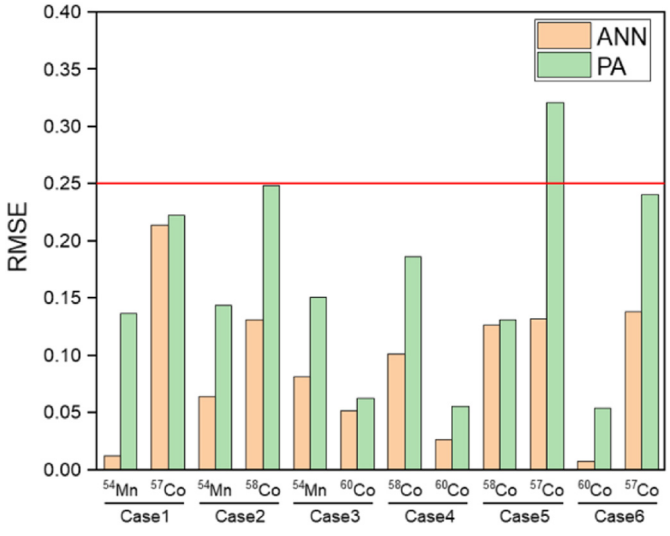

Fig. 7. Comparison results of the RMSE values resulting from the ANN and PA method.

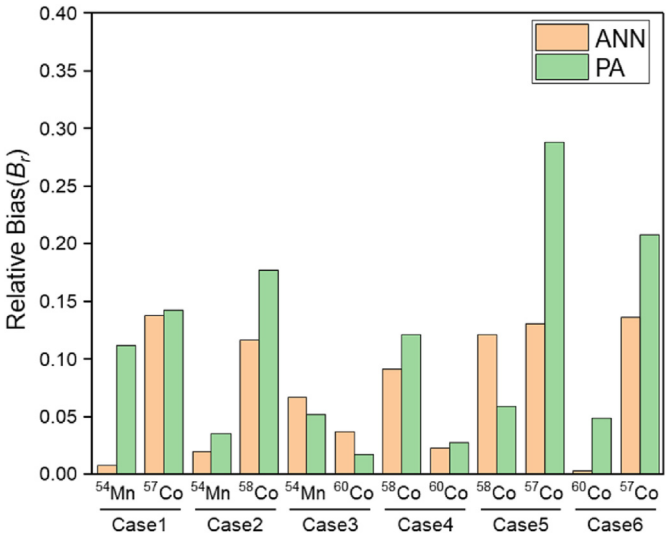

Fig. 8. Comparison of the relative bias (B_r) values resulting from the ANN and PA method.

i) High-energy gamma ray emitter with photopeaks that are not overlapped by those of interfering RIs

In cases that included ^{60}Co, a high-energy gamma ray emitter, both the ANN and PA method show the lowest RMSE values, as shown in Fig. 7. In Cases 3,4, and 6, the maximum RMSE of the ANN

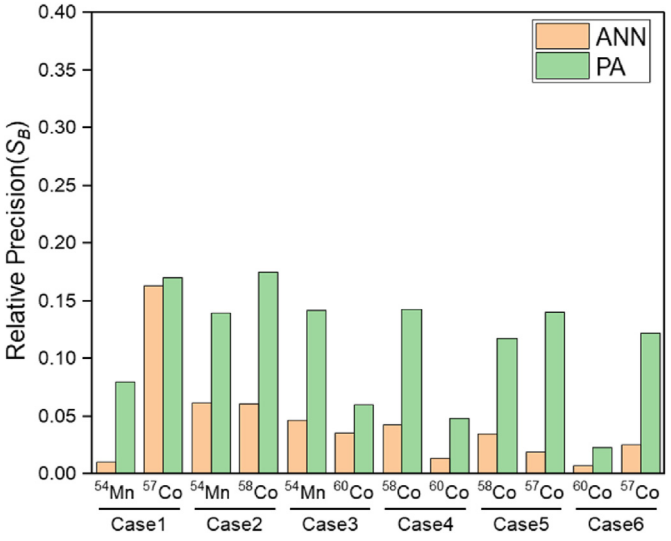

Fig. 9. Comparison of the relative precision (S_B) values resulting from the ANN and PA method.

Table 7
RMSE values derived from the ANN and PA method.

Case	RI	RMSE		RI	RMSE	
		ANN	PA		ANN	PA
1	^{54}Mn	0.013	0.137	^{57}Co	0.214	0.223
2	^{54}Mn	0.065	0.144	^{58}Co	0.131	0.249
3	^{54}Mn	0.082	0.151	^{60}Co	0.052	0.063
4	^{58}Co	0.101	0.187	^{60}Co	0.027	0.055
5	^{58}Co	0.126	0.132	^{57}Co	0.132	0.321
6	^{60}Co	0.008	0.054	^{57}Co	0.138	0.241

and PA method for ^{60}Co are only 0.052 and 0.063, respectively, which are quite low compared to the criterion, and the ANN shows better performance (lower values) than the PA method. In Figs. 8 and 9, the ANN also shows lower B_r and S_B values than the PA method with the exception of the B_r value of Case 3 for ^{60}Co.

In the case of ^{60}Co, the photopeaks at 1.17 MeV and 1.33 MeV do not overlap with those of ^{134}Cs and ^{137}Cs, as shown in Fig. 3. Therefore, it is not difficult to differentiate and quantify ^{60}Co using either the ANN or PA when interfering RIs, ^{134}Cs and ^{137}Cs, are present.

ii) Medium-energy gamma ray emitters with photopeaks that are overlapped by those of interfering RIs

In cases that included ^{54}Mn or ^{58}Co, the photopeaks of the two gamma ray emitters are partially overlapped by those of ^{134}Cs. The 835 keV photopeak of ^{54}Mn is overlapped by the 796 keV photopeak of ^{134}Cs, and the 511 and 811 keV photopeaks of ^{58}Co are overlapped by the 605 and 796 keV photopeaks of ^{134}Cs, respectively. These overlapping peaks result from the inferior resolution of the NaI(Tl) detectors of the FastScan. However, the 662 keV photopeak of ^{137}Cs does not overlap with the peaks of the four RIs that were tested, as shown in Fig. 3. In these cases, the performance of the ANN developed in this study is superior to that of the PA method except for ^{58}Co in Case 5. The RMSE values of the ANN for ^{54}Mn and ^{58}Co range from 0.013 to 0.137, whereas those of the PA method range from 0.132 to 0.249:

- In Case 1, the RMSE value of the ANN for ^{54}Mn is about 14 times lower than that of the PA method. In addition, the B_r, and S_B values of the ANN are 8 and 10 times lower, respectively, than those of the PA method, as shown in Figs. 8 and 9.
- In Cases 2, 3, and 4, the RMSE values of the ANN for ^{54}Mn or ^{58}Co are about 2 times lower than those of the PA method. In particular, for ^{58}Co in Case 2, the RMSE value (0.131) of the ANN is considerably smaller than that of the PA method (0.249), which is very close to the criterion. As shown in Figs. 8 and 9, the B_r and S_B values of the ANN are 1.3–3.4 times lower than those of the PA method except for the B_r value for ^{54}Mn in Case 3.
- In Case 5, for ^{58}Co, the RMSE values of ANN and PA are 0.126 and 0.132, respectively, revealing little discrepancy between the two methods. In this case, the B_r value of the ANN is 2 times higher than that of the PA method while the S_B value of the ANN is about 3.4 times lower than that of the PA method.

For ^{54}Mn and ^{58}Co, the ANN is less susceptible to photopeak interference than the PA method. The superior performance of the ANN may result from the fact that the ANN uses the features of the entire spectra to identify and quantify the RIs while the PA method uses only the photopeak regions of the spectra.

iii) Low-energy gamma ray emitters with photopeaks located in the low-energy region of the Compton continuum of interfering RIs

Obtaining accurate low-energy spectrometry (below 300 keV) using the NaI(Tl) detector has been challenging due to the Compton continuum resulting from RIs with gamma ray energy exceeding 300 keV [12,13]. In addition, the energy range of the FastScan, according to the specification sheet from Canberra Inc., ranges from 300 keV to 1.8 MeV. In cases that included ^{57}Co, its 122 and 136 keV photopeaks may face interference from the Compton continuum of the interfering RIs, ^{134}Cs and ^{137}Cs. In addition, its two photopeaks appear as one entity which does not show a Gaussian shape due to the low resolution of the NaI(Tl) detectors, as seen in Fig. 3. In Cases 1, 5, and 6, the RMSE values for ^{57}Co derived by the ANN are within the criterion, but those of the PA method are very close to or exceed it:

- In Case 1, the ANN and PA method produced similar RMSE values, 0.214 and 0.223, respectively for ^{57}Co. The RMSE value of 0.214 is the highest value produced by the ANN in this study. Not only the RMSE value but also the B_r and S_B values for ^{57}Co are similar between the ANN and PA method, as shown in Figs. 8 and 9.
- In Case 5, the RMSE value of the ANN for ^{57}Co is 0.132 while that of the PA method is 0.321, which exceeds the criterion. This is attributable to the lower B_r and S_B values of the ANN than the PA method. As shown in Fig. 8, the B_r value of the PA method for ^{57}Co is 0.289, which greatly exceeds the criterion irrespective of the S_B value.
- In Case 6, the RMSE value of the ANN for ^{57}Co is about 1.7 times lower than that of the PA method, which is very close to the criterion. In addition, the B_r and S_B values of the ANN are 0.136 and 0.026, respectively, which are lower than those of the PA method.

Although the FastScan uses NaI(Tl) detectors, the performance of the ANN in this study satisfies the criterion when the low-energy photopeaks (122 and 136 keV) of ^{57}Co are located in the Compton continuum of the interfering RIs. For the same case, however, the PA method shows inferior performance as the RMSE values are very close to or exceed the criterion. Because the peak shape of ^{57}Co is not Gaussian, fitting the photopeak using a Gaussian function seems to contribute to the observed higher B_r values compared to those of the other RIs, as shown in Fig. 8. On the other hand, the ANN shows promise in quantifying the RIs that emit low-energy gamma rays below 300 keV with non-Gaussian photopeaks.

When applying the ANN to the FastScan data, all of the resulting RMSE values for the lung configuration meet the criterion and are less than those derived from the PA method. Thus, the performance of the FastScan to measure intake of RIs in lung could be improved through use of the ANN.

4. Conclusion

In order to improve the performance of the FastScan in the lung configuration of the fission and activation products category given in the ANSI/HPS 13.30–2011, we developed an ANN and compared its performance with that of the PA method which is currently used for identification and quantification of RIs. On the whole, the ANN showed superior performance even when the photopeaks of the analytes overlapped those of the interfering RIs or there was a low-energy photopeak below 300 keV. All of the RMSE values derived from the ANN were within the criterion (RMSE $\leq$0.25), while three of those derived from the PA method exceeded or were very close to it. Among the twelve RMSE values of the ANN, nine were about 2–10 times less than those of the PA method and the other three were slightly less than those of the PA method. By using the ANN, therefore, the performance of the FastScan in the lung configuration can be improved to meet the criterion despite the low resolution of the NaI(Tl) detector. In addition, using the quantification method proposed in this study, the output of the ANN, which is a relative activity contribution, can be converted to an absolute measure of the activity of a single RI. However, the maximum RMSE value of the ANN was 0.214, which did not show a sufficient margin to the criterion.

In future, we plan to develop an ANN focusing on the other five categories of the lung configuration given in ANSI/HPS 13.30–2011. These include X-ray and low-energy gamma emitters, ^{238}Pu, ^{241}Am,

^{234}Th, ^{235}U, and ^{237}Np. Because the ANN showed promise for analysis of the low-energy gamma ray emitter ^{57}Co, further improvement in the FastScan is expected through development of an ANN only for low-energy gamma emitters. In addition, we will apply other machine learning methods such as convolutional neural network (CNN) in order to minimize the RMSE values of the FastScan. In 2021, KHNP-CRI plans to apply the ANN to the three NPPs which did not meet the criterion in 2018 and to compare its performance with the previous results.

Declaration of competing interest

The authors declare that they have no known competing financial interests or personal relationships that could have appeared to influence the work reported in this paper.

References

[1] Health Physics Society, Performance Criteria for Radiobioassay, ANSI/HPS N13.30-2011, 2011. https://global.ihs.com/doc_detail.cfm?document_name=ANSI%2FHPS%20N13%2E30&item_s_key=00215007.
[2] Jung Kwon Son, Tae Young Kong, Siyoung Kim, Improvement of the Performance Test Method for In-Vivo/vitro Measurement Equipment, Korea Hydro & Nuclear Power., LTD, 2019.
[3] M. Kamuda, J. Stinnett, C.J. Sullivan, Automated isotope identification algorithm using artificial neural networks, IEEE Trans. Nucl. Sci. 64 (2017) 1858–1864, https://doi.org/10.1109/TNS.2017.2693152.
[4] M. Kamuda, C.J. Sullivan, An automated isotope identification and quantification algorithm for isotope mixtures in low-resolution gamma-ray spectra, Radiat. Phys. Chem. 155 (2019) 281–286, https://doi.org/10.1016/j.radphyschem.2018.06.017.
[5] J. Kim, K.T. Lim, J. Kim, C. jong Kim, B. Jeon, K. Park, G. Kim, H. Kim, G. Cho, Quantitative analysis of NaI(Tl) gamma-ray spectrometry using an artificial neural network, Nucl. Instruments Methods Phys. Res. Sect. A Accel. Spectrometers, Detect. Assoc. Equip. 944 (2019) 162549, https://doi.org/10.1016/j.nima.2019.162549.
[6] P. Olmos, J.C. Diaz, J.M. Perez, P. Aguayo, A. Bru, G. Garcia-Belmonte, J.L. de Pablos, P. Gomez, V. Rodellar, A new approach to automatic radiation spectrum analysis, IEEE Trans. Nucl. Sci. 38 (1991) 971–975, https://doi.org/10.1109/23.83860.
[7] FASTSCAN High-Throughput Whole Body Counter, Mirion Technol., 2019. https://www.mirion.com/products/2250-fastscan-high-throughput-whole-body-counter.
[8] O.R. Perry, Calibration of the Accuscan-II In-Vivo System for I-125 Thyroid Counting, Appendix J, 2011.
[9] F. Chollet, Deep Learning with Python, Manning Publications Co., 2017, pp. 8–97.
[10] S. Alla, S.K. Adari, Beginning Anomaly Detection Using Python-Based Deep Learning, Apress, 2019, https://doi.org/10.1007/978-1-4842-5177-5.
[11] Genie, Spectroscopy Software Customization Tools, 9233653J V3.4, Canberra Inc., 2000.
[12] K. Saito, S. Moriuchi, Monte Carlo calculation of NaI(Tl) detector response functions for low energy gamma rays, Nucl. Instrum. Methods Phys. Res. A. 226 (1984) 449–454, https://doi.org/10.1016/0168-9002(84)90063-9.
[13] J. Plagnard, C. Hamon, M.C. Lépy, Study of scattering effects in low-energy gamma-ray spectrometry, Appl. Radiat. Isot. 66 (2008) 769–773, https://doi.org/10.1016/j.apradiso.2008.02.016.